Eur. Phys. J. B **60**, 319–324 (2007)
DOI: 10.1140/epjb/e2007-00348-3

THE EUROPEAN PHYSICAL JOURNAL B

Variable-range hopping in $Fe_{70}Pt_{30}$ catalyzed multi-walled carbon nanotubes film

M. Aggarwal[1], S. Khan[1,2], M. Husain[1,a], T.C. Ming[3], M.Y. Tsai[3], T.P. Perng[3], and Z.H. Khan[4]

[1] Department of Physics, Jamia Millia Islamia, New Delhi-110025, India
[2] Department of Electronic Science, University of Delhi South Campus, New Delhi-110021, India
[3] Department of Materials Science and Engineering & Department of Physics, National Tsing Hua University, Hsinchu, Taiwan
[4] Department of Applied Sciences & Humanities, Jamia Millia Islamia (Central University), New Delhi-110025, India

Received 25 January 2007 / Received in final form 30 May 2007
Published online 22 December 2007 –

Abstract. Using low-pressure chemical vapour deposition (LPCVD), multi-walled carbon nanotubes (MWNTs) are grown on nanocrystalline $Fe_{70}Pt_{30}$ film. The $Fe_{70}Pt_{30}$ nanocrystalline film is deposited by vapour condensation technique. The size of the nanoparticles varies from 5–10 nm, as inferred from SEM micrographs of $Fe_{70}Pt_{30}$ film. SEM and TEM observations of as-grown CNTs film reveal that these are multi-walled and their diameter varies from 30–80 nm and length is of the order of several micrometers respectively. There is a structural change from ordinary geometry of CNTs to bamboo shaped as suggested by TEM image. Raman spectra shows sharp G and D bands with a higher intensity of G band showing the presence of graphitic nature of the nanotubes. An experimental study of the temperature dependence of electrical conductivity of MWNTs film is done over a wide temperature range from (293–4 K). The measured data gives a good fit to variable-range hopping (VRH) and the results are interpreted using Mott's (VRH) model. The conduction mechanism of the MWNTs film shows a crossover from the $\exp\left[-(T_o/T)^{1/4}\right]$ law in the temperature range (293–110 K) to $\exp\left[-(T_m/T)^{1/3}\right]$ in the low temperature range (110–4 K). This behaviour is attributed to temperature-induced transition from three-dimension (3D) to two-dimension (2D) VRH. Various Mott's parameters like characteristic temperature (T_m), density of states at Fermi level $N(E_F)$, localization length (ξ), hopping distance (R), hopping energy (W) have also been calculated using above-mentioned model.

PACS. 68.37.Hk Scanning electron microscopy (SEM) (including EBIC) – 68.37.Lp Transmission electron microscopy (TEM) (including STEM, HRTEM, etc.) – 73.63.Fg Nanotubes – 73.23.Ad Ballistic transport

1 Introduction

With the discovery of carbon nanotube (CNT) structures by Iijima [1], a new class of materials with a reduced dimensionality has been introduced. Carbon nanotubes (CNTs) have thus, attracted great interest due to their remarkable structural, electrical and mechanical properties and their wide range of potential for nano-electronic device applications [2]. The strong influence of the structural parameters viz. diameter, helicity and number of concentric cylinders on the band structure [3] results in unusual electrical transport properties. Multi-walled and single-walled carbon nanotubes are thus, found to be interesting systems, where different aspects of electrical conduction are observed. In clean metallic single-walled carbon nanotubes (SWNTs), the electron transport is ballistic [4,5] whereas some groups [6–8] have reported that the multi-walled carbon nanotubes (MWNTs) also exhibit ballistic conduction. Reports [9–11] on the diffusive conduction characteristics of MWNTs are also available in the literature. The electrical transport mechanism in carbon nanotubes can also be interpreted in terms of variable-range hopping (VRH) conduction. During the last three decades, the growing interest in the hopping transport has followed in the footsteps of the development of physics of disordered systems. In disordered systems, Mott [12] has developed the concept of variable–range hopping (VRH) of localized electrons between the different sites. The conduction process thus, involves the electron hop between localized states with energy as low as possible. These states are kept far from each other involving certain distance (hopping length), which increases with the decreasing temperature, which gives rise to the origin of 'variable-range hopping (VRH)'. It is seen that the dependence of temperature on the electrical conductivity in the VRH regime is given by $\sigma(T) = \sigma_0 \exp[-(T_0/T)]^a$, where σ is the electrical conductivity, T is the temperature, σ_0 and T_0 are the constants, and $a = 1/3, 1/4$ for non–interacting

[a] e-mail: mush_reslab@rediffmail.com

two-dimensional (2D) and three-dimensional (3D) systems, respectively.

In the literature, reports [13–16] are available on the electrical transport properties of carbon nanotubes. The low temperature transport measurements of bulk samples of carbon multilayer nanotubes with a structure of nested cones, was studied by Tsebro et al. [17]. Their results were interpreted in terms of two-dimensional variable-range hopping. Tsigankov et al. [18] have reported the temperature dependence of conductivity and variable-range hopping in two-dimensional system. Yosida et al. [19] has observed the phenomenon of VRH during the growth of sheets (7–92 μm in thickness) composed of multi-walled carbon nanotubes and electrical resistance was studied in the temperature range ($7 < T < 300$ K). The calculated hopping length was $\cong 0.16$ μm. Keeping in view of the above, it is important to study such complex systems in order to get more information about the electrical conduction mechanism. In the present research work, we have studied the electrical conduction mechanism of $Fe_{70}Pt_{30}$ catalysed multi-walled carbon nanotubes film using Mott's variable-range hopping model.

2 Experimental

Initially, the $Fe_{70}Pt_{30}$ alloy was prepared by arc-discharge method. After the arc-discharge, the ignots of $Fe_{70}Pt_{30}$ were collected and were used to synthesize the $Fe_{70}Pt_{30}$ nanocrystalline film on silicon substrate using vapour condensation technique. This nanocrystalline film was then used as a catalyst to grow CNTs by a low-pressure chemical vapour deposition (LPCVD) method. Using this method, CNTs were successfully grown on a $Fe_{70}Pt_{30}$ supported catalyst film. During this process, the chamber pressure and the temperature were maintained at 10 Torr and 800 °C respectively. A gas mixture of N_2:C_2H_2:H_2 with flow rates 300:50:50 sccm respectively, were made to flow through mass flow controllers (MFC's) into the chamber of LPCVD. For the growth of CNTs, the growth time was kept fixed at 30 min. The morphology and microstructure of as-grown CNTs film were investigated by Scanning Electron Microscope (SEM) and Transmission Electron Microscope (TEM). To confirm the diameter and wall structure of this multi-walled carbon nanotubes (MWNTs) film, HRTEM investigation was also performed. Fourier Transform Raman Spectrometer was also employed to verify the graphitic nature of these nanotubes. This spectrometer involves the use of Nd:YAG laser with an excitation wavelength of 1064 nm. We have used four-probe method to measure the electrical transport properties of this MWNTs film. For this method, the contacts on MWNTs film were made by using four platinum wires. These platinum wires were pasted with the help of silver paste and the distance between each contact was kept fixed at 4 mm. A specially designed sample holder with standard lock-in technique was used to measure R–T curves for the temperature range (293–4 K).

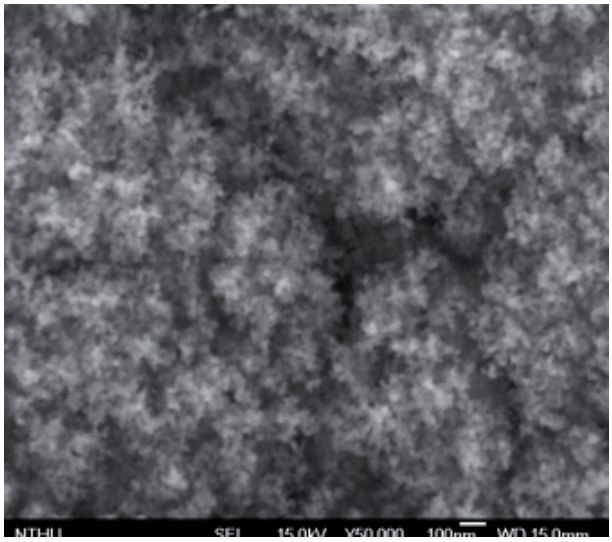

Fig. 1. SEM image of $Fe_{70}Pt_{30}$ nanocrystalline film.

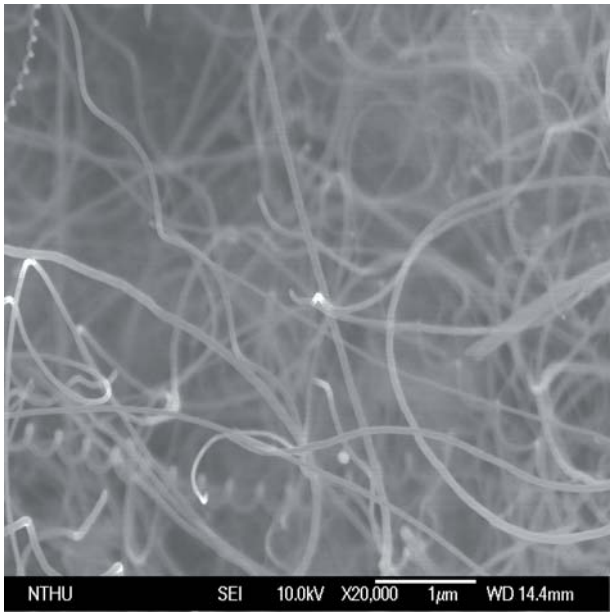

Fig. 2. SEM image of $Fe_{70}Pt_{30}$ catalyzed Multi-walled Carbon Nanotubes Films (MWNTs).

3 Results and discussion

It is evident from the SEM image of nanocrystalline $Fe_{70}Pt_{30}$ film that the size of these nanoparticles varies from 5–10 nm (Fig. 1). SEM image of as–grown CNTs on $Fe_{70}Pt_{30}$ catalysed film is presented in Figure 2. It also suggests that the average diameter of these nanotubes varies from 30–80 nm and length is of the order of several micrometers respectively. The TEM image (Fig. 3) indicates that CNTs grown are multi-walled and bamboo-shaped. Figure 4 presents the HRTEM image of as-grown MWNTs. From this Figure, it is revealed that the diameter of the central hollow portion of the MWNT is about 10 nm and wall thickness is about 12 nm. The graphite layer lattice fringes are somewhat broken but parallel to

Fig. 3. TEM image of as-grown MWNTs.

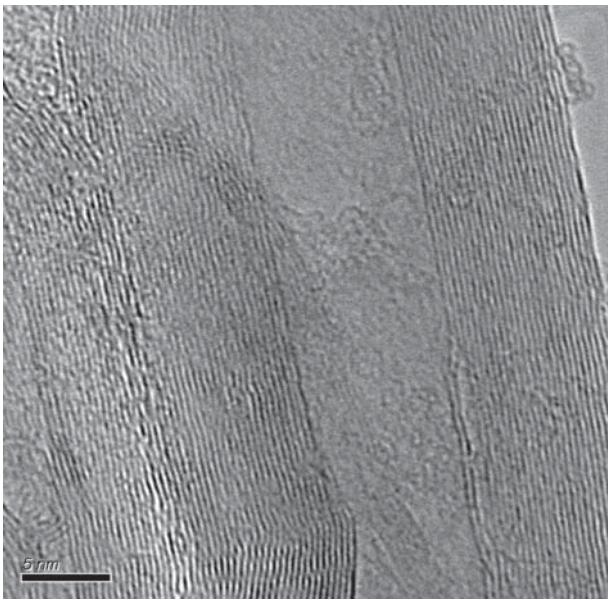

Fig. 4. HRTEM image of as-grown MWNTs.

the tube axis. The formation of bamboo–shaped carbon nanotube involves a) the decomposition of the hydrocarbon molecule at the surface of the catalyst b) dissolution of the carbon atoms into the metal forming a solid solution. When this solution gets supersaturated, carbon atoms diffuse through the bulk of the particle and precipitates at its surface in the form of crystalline graphitic layers. It is seen that the films grown on bimetallic catalyst (here Fe–Pt), the density and purity of MWNTs is significantly more in comparison with those grown on mono-metallic

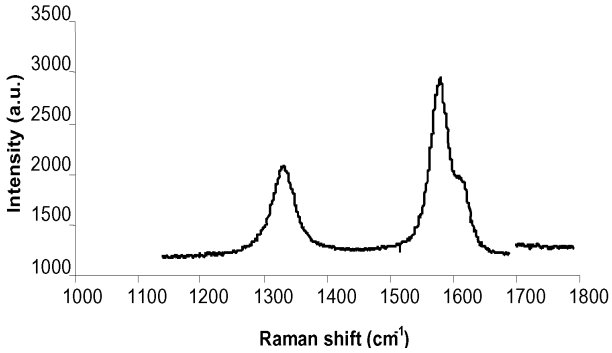

Fig. 5. Raman Spectra of MWNTs.

catalyst. The use of bi-metallic coatings eventually eliminates the formation of residual Fe_3C catalyst particle at the tip of nanotube [20]. It also enhances hydrocarbon conversion to filamentous carbon or carbonaceous solids. Various bi-metallic catalysts have been used in the decomposition of ethylene to produce methane, ethane and solid carbon [21–23] to prepare carbon filaments [24,25]. Thus, the higher yield of CNTs with bi-metallic catalysts has been attributed to particle melting point reduction, increase in the carbon solubility and the formation of well-dispersed metal clusters upon segregation during CNT formation [26,27]. Here, we have also performed Raman spectroscopy of as-grown MWNTs, shown in Figure 5. Normally, the Raman spectra is sensitive for minor changes inside the carbon layers. A peak centered at $\sim$1340 cm^{-1}, which is called as D band indicates defects and impurities inside the carbon layers, while, a peak located at $\sim$1580 cm^{-1} is called as G band [28,29]. In the present system, G band is at higher intensity, indicating that the CNTs are graphitized.

Electrical transport properties are the basis for electronics and are exceptionally important to understand in detail. In this section, we study the mechanism for the electrical transport characteristics of multi-walled carbon nanotubes (MWNTs) grown on $Fe_{70}Pt_{30}$ catalysed nanocrystalline film. To elucidate the mechanism of transport in the present system, the conductivity (σ) is measured over the entire temperature range (293–4 K) and its temperature dependence is shown in Figure 6. This figure clearly indicates the decrease in conductivity with the decrease in temperature. Such kind of behaviour was observed in both MWNTs and SWNTs, where the temperature dependence was fitted to a power-law function. For MWNTs, this behaviour was explained in terms of Luttinger liquid (LL) model [30]. A key manifestation of the presence of LL state is the existence of a power-law dependence of the tunneling conductance on temperature. Other mechanisms like thermally activated transport ($\ln G(T) \propto -1/T$), weak localization ($G(T) \propto \ln T$ [31]) and variable-range hopping (VRH) [32], that suppress the conductance at lower temperatures, were also considered. However, in the present system, we have found that VRH model gives a good fit to our data.

Various authors [32] have reported that at low temperatures, the transfer of electrons between the nearest

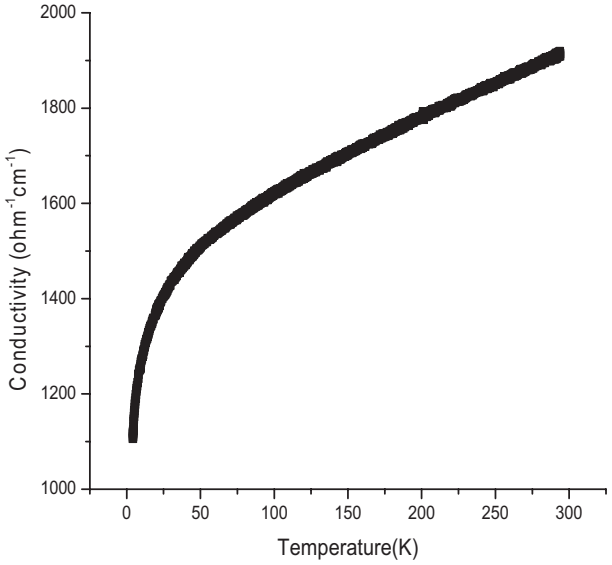

Fig. 6. Conductivity (σ) vs. temperature (T) plot for MWNTs film.

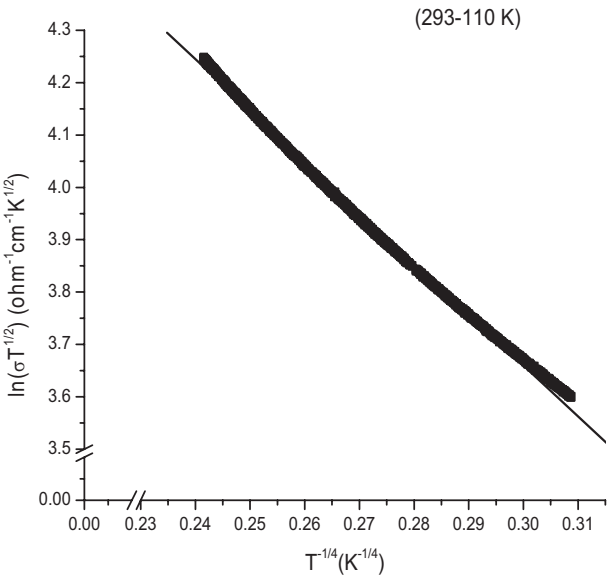

Fig. 7. $\ln(\sigma\sqrt{T})$ vs. $T^{-1/4}$ plot for MWNTs film.

neighbour sites may be less favoured than that of more distant sites of energetically accessible states, which ultimately reduces the energy necessary for the transition. Therefore, for disordered systems, the low temperature transport is governed by variable-range hopping (VRH) between the localized states. Mott [33] predicted, for the first time, the key relation for the temperature dependence of conductivity for non-interacting carriers and for a constant density of states near the Fermi energy (a slowly varying function of energy). At low temperatures, it was concluded by Mott [33] that the electrons seek accessible energy states by hopping distances beyond the localization length, leading to the variable-range hopping (VRH) mechanism.

On the basis of the above-mentioned Mott's theory, we have also tried to explain the conduction mechanism with the help of Mott's VRH model in the present system. This model describes the electronic conduction in a disordered system [34–37], where the electronic wave function becomes strongly localized due to disorderness.

Figure 7 shows a plot of $(\ln(\sigma\sqrt{T})$ vs. $(T^{-1/4})$, where all the data points lie on a straight line over the temperature range (293–110 K). This behaviour indicates variable-range hopping (VRH) by a tunneling process near Fermi level.

According to Mott [33], conductivity (σ) is given as:

$$\sigma = \frac{\sigma_0'}{\sqrt{T}} \exp(-AT^{-1/4}) \tag{1}$$

where,

$$A^4 = T_0 = \frac{\lambda\alpha^3}{k_B N(E_F)} \tag{2}$$

$N(E_F)$ is the density of localized states at E_F, λ is a dimensionless constant (about 18), α^{-1} represents the spatial extension of the wave function $\exp(-\alpha R)$ associated with the localized states, T_0 is the degree of disorder and k_B is the Boltzmann constant. The value of σ_0 as obtained by various workers is given by:

$$\sigma_0' = 3e^2\gamma \left\{\frac{N(E_F)}{8\pi\alpha k\mathrm{T}}\right\}^{1/2} \tag{3}$$

where, e is the electron charge and γ is Debye frequency (about 10^{13} Hz)

On solving (2) and (3),

$$\alpha = 22.52\sigma_0' A^2 \text{ cm}^{-1} \tag{4}$$

and

$$N(E_F) = 2.12 \times 10^9 \sigma_0'^3 A^2 \text{ cm}^{-3}\text{eV}^{-1}. \tag{5}$$

The hopping distance [33] is given by:

$$R = \left(\frac{9}{8\pi\alpha k\mathrm{T}N(E_F)}\right)^{1/4}. \tag{6}$$

Hopping energy [33] is given by:

$$W = \left(\frac{3}{4\pi R^3 N(E_F)}\right). \tag{7}$$

Using equations (1)–(7), various Mott's parameters like σ_0', $N(E_F)$, T_0, α, W and αR are calculated (presented in Tab. 1). According to Mott, the values of W should be of the order of kT and that of αR should be of the order of/greater than unity. The calculated value of density of states near the Fermi level obtained using Mott's VRH relations comes out to be 7.55×10^{19} eV^{-1} cm^{-3}. Various workers [38–40] have reported the bulk density of states $\sim 10^{18}$ eV^{-1} cm^{-3} for amorphous carbon films. For one–layer carbon nanotube film, the density of states [17] at Fermi level was reported to be $\sim 10^{21}$ eV^{-1} cm^{-3}. In the present system, value of $N(E_F)$ is of the same order as reported by earlier workers.

Table 1. The Mott parameters for $Fe_{70}Pt_{30}$ catalyzed MWNTs film for the temperature range (293–110 K).

Temperature T (K)	Density of localized states at E_F $N(E_F)$ ($eV^{-1}cm^{-3}$)	Spatial extension associated with localized states $\alpha(cm^{-1})$	Hopping distance R (cm)	Hopping energy W (meV)	αR
293	7.55×10^{19}	1.54×10^{6}	5.9×10^{-7}	15.4	0.91
250	7.55×10^{19}	1.54×10^{6}	6.1×10^{-7}	13.9	0.94
200	7.55×10^{19}	1.54×10^{6}	6.5×10^{-7}	11.7	0.99
150	7.55×10^{19}	1.54×10^{6}	7.0×10^{-7}	9.4	1.08

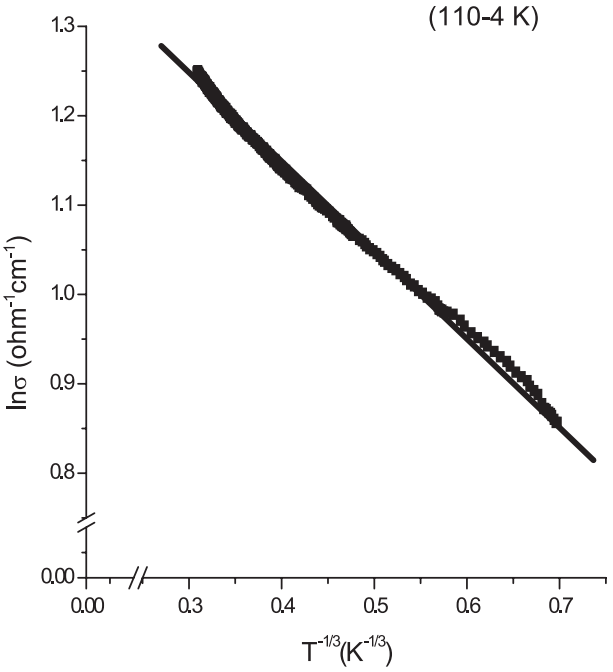

Fig. 8. $\ln\sigma$ vs. $T^{-1/3}$ plot for MWNTs film.

Table 1 shows that, the hopping distance (R) increases as the temperature decreases from 293 to 110 K. The calculated value of T_0 comes out to be 0.14×10^4 K. The large value of T_0 shows that the localization of carriers in this system is strong, i.e., the system may be disordered. Several workers [41] have reported the value of $T_0 \approx 10^4$ K for plasma polymerized C_{60} thin films and on the basis of the value of T_0, they concluded that their system is disordered. In our case, the value of T_0 is of the same order as that of reported by these workers. The calculated values of W are of the order of kT and that of αR are of the order of/greater than unity, which is in agreement with Mott's condition of variable–range hopping.

For the lower temperature region (110–4 K), a plot of ln σ vs. $T^{-1/3}$ shows a straight line as presented in Figure 8. This indicates that the conductivity scales as $\exp\left[(-1/T)^{1/3}\right]$ suggesting that the conduction is in the two–dimensional (2D) non–interacting VRH regime. On the basis of this model, we have estimated the localization length and the optimum hopping distance for the present system.

Our experimental data fits to the plot of ln σ vs. $T^{-1/3}$ (Fig. 8), and conductivity (σ) obeys the following relation:

$$\sigma\sqrt{T} = \sigma_0 \exp\left[-\left(\frac{T_m}{T}\right)^{1/3}\right]. \tag{8}$$

In two–dimensional variable–range hopping regime, the characteristic temperature (T_0) is related to the density of states at the Fermi level $N(E_F)$ and the localization ξ as [35];

$$T_m = \frac{13.8}{k_B N(E_F)\xi^2}. \tag{9}$$

The temperature dependence of optimum hopping distance is given by [16];

$$R(T) = \frac{1}{3}\xi\left(\frac{T_m}{T}\right)^{1/3}. \tag{10}$$

Using relations (9) and (10), it is possible to estimate the localization length and the optimum hopping distance. The density of localized states in two-dimension (2D) ($N_{2D}(E_F)$) can be calculated by multiplying the value of ($N(E_F)$) obtained using 3D VRH with the film thickness, as suggested by earlier workers [42]. Using this, localization length comes out to be 0.63×10^{-6} cm. The optimum hopping distance at 110 K and 4 K is estimated to be 0.04×10^{-6} cm and 0.13×10^{-6} cm respectively.

4 Conclusion

Bamboo-shaped MWNTs were grown on $Fe_{70}Pt_{30}$ catalysed nanocrystalline film and the diameter of these nanotubes varied from 30–80 nm and length is of the order of several micrometers respectively. The temperature dependence of conductivity of MWNTs film for the temperature range (293–4 K) indicated that the main contribution to the conductivity came from the carriers that hop via variable-range hopping (VRH). Three-dimensional (3D) VRH was observed in the temperature range 293–110 K. On the basis of the values of W and αR, it is concluded that the conduction is due to variable–range hopping, which follows the Mott's variable-range hopping model. Below 110 K i.e. for $110 < T < 4$ K, the data was well fitted to Mott's two-dimensional (2D) VRH. Using this model, the value of localization length comes out to be 0.63×10^{-6} cm and the hopping distance at low temperature (4 K) was estimated to be 0.13×10^{-6} cm.

References

1. S. Iijima, Nature (London) **354**, 56 (1991)
2. Z.H. Khan, M. Husain, Ind. Journ. Engg. Mater. Sci. **12**, 529 (2005)
3. R. Saito, G. Dresselhaus, M.S. Dresselhaus, Imperial College Press London (1998)
4. A. Bachtold, M.D. Jonge, K.G. Rasmussenn, P.L. McEuen, Phys. Rev. Lett. **87**, 166801 (2001)
5. W.J. Liang, M. Bockrath, D. Bozovic, J.H. Hafner, M. Tinkham, H. Park, Nature **411**, 665 (2001)
6. P.J. de Pablo, E. Graugnard, B. Walsh, R.P. Andres, S. Datta, R. Reijenberger, Appl. Phys. Lett. **74**, 323 (1999)
7. C. Bergem, Y. Yi, Z.I. Wang, W.A. de Heer, Appl. Phys. A **74**, 363 (2002)
8. P. Poncharal, C. Berger, Y. Yi, Z.L. Wang, W.A. de Heer, J. Phys. Chem. B **106**, 12104 (2002)
9. A. Bachtold, M. Henny, C. Terrier, C. Strunk, C. Schonenberger, J.P. Salvetat, J.M. Bonard, L. Forro, Appl. Phys. Lett. **73**, 274 (1998)
10. A. Bachtold, M.S. Fuhrer, S. Plyasunov, M. Forero, E.H. Anderson, A. Zettle, P.L. Mc Euen, Phys. Rev. Lett. **84**, 6082 (2000)
11. C. Schonenberger, A. Bachtold, C. Strunk, H.P. Salvetat, L. Forro, Appl. Phys. A **69**, 283 (1999)
12. N. Mott, J. Non-Cryst. Solids **1**, 1 (1968)
13. E.S. Choi, J.S. Brooks, D.L. Eaton, M.S. Al-Haik, M.Y. Hussaini, H. Garmestani, D. Li, K. Dahmen, J. Appl. Phys. **94**, 6034 (2003)
14. W. Bingqing, R. Spolenak, P.K. Redlich, M. Ruhle, E. Arzt, Appl. Phys. Lett. **74**, 3149 (1999)
15. G.U. Sumanasekera, C. Adu, P.C. Eklund, Phys. Rev. Lett. **85**, 1096 (2000)
16. L. Grigorian, G.U. Sumanasekera, A.L. Loper, P.C. Eklund, Phys. Rev. B **58**, R4195 (1998)
17. V.I. Tsebro, O.E. Omel'yanovskii, E.F. Kukovitskii, N.A. Sainov, N.A. Kiselev, D.N. Zakharov, JETP **86**, 1216 (1998)
18. D.N. Tsigankov, A.L. Efros, Cond. Matt. **88**, 176602-1 (2002)
19. Y. Yosida, J. Phys. Chem. Solids **60**, 1 (1999)
20. M. Mayne, N. Grobert, M. Terrones, R. Kamalakaran, M. Ruhle, H.W. Kroto, Chem. Phys. Lett. **338**, 101 (2001)
21. C. Park, R.T.K. Baker, J. Catal **179**, 361 (1998)
22. C. Park, R.T.K. Baker, J. Catal. **190**, 104 (2000)
23. P.E. Anderson, N.M. Rodriguez, Chem. Mater. **12**, 823 (2000)
24. M. Audier, J. Guinot, M. Coulon, L. Bonnetain, Carbon **19**, 99 (1981)
25. A. Sacco, Series E: Applied Sciences **177** (1990) Dordrecht: Kluwer
26. A.M. Cassell, J.A. Raymakers, J. Kong, Daih, J. Phys. Chem. B **103**, 6484 (1999)
27. J.E. Herrera, L. Balzano, A. Borgna, W.E. Alvarez, D.E. Resasco, J. Catal. **204**, 129 (2001)
28. J. Schwan, S. Ulrich, V. Batoriv, H. Ehrhardt, J. Appl. Phys. **80**, 1 (1996)
29. H. Murphy, P. Papakonstantinou, T.I. Okpalugo, J. Vac. Sci. Technol. B **24**, 2 (2006)
30. R. Egger, Phys. Rev. Lett. **83**, 5547 (1999)
31. L. Langer, V. Bayot, E. Grivei, J.-P. Issi, J.P. Heremans, C.H. Olk, L. Stockman, C. Van Haesendonck, Y. Bruynseraede, Phys. Rev. Lett. **76**, 479 (1996)
32. Y.H. Lee, D.H. Kim, H. Kim, B.K. Ju, J. Appl. Phys. **88**, 4181 (2000)
33. N.F. Mott, E.A. Davis, *Electronic Processes in Non-Crystalline Materials* (Oxford, Clarendon, 1970)
34. N.F. Mott, *Conduction in Non-Crystalline Materials* (Oxford University Press, Oxford, 1987)
35. B.I. Shklovskii, A.L. Efros (Electronic Properties of Doped Semiconductors Springer, Berlin, 1984)
36. E.B. Maiken, P. Taborek, J. Appl. Phys. **87**, 9 (2000)
37. C.A. Dimitriadis, N.A. Hastas, N. Vouroutzis, S. Logothedis, Y. Panayiotatos, J. Appl. Phys. **89**, 12 (2001)
38. J.J. Hauser, J. Non-Cryst. Solids **23**, 21 (1977)
39. Th. Frauenheim, U. Stephan, K. Bewilogua, F. Jungnickel, P. Blaudeck, E. Fromm, Thin Solid Films **182**, 63 (1989)
40. C. Godet, Philosophical Magazine B **81**, 205 (2001)
41. M. Shiraishi, M. Ramm, M. Ata, Appl. Phys. A 613 (2002)
42. W.Y. Jang, N.N. Kulkarni, C.K. Shih, Y. Zhen, Appl. Phys. Lett. **84**, 1177 (2004)